Science Advances
AAAS

advances.sciencemag.org/cgi/content/full/6/29/eaba9589/DC1

Supplementary Materials for

Cell invasion in digital microfluidic microgel systems

Bingyu B. Li, Erica Y. Scott, M. Dean Chamberlain, Bill T. V. Duong, Shuailong Zhang, Susan J. Done, Aaron R. Wheeler*

*Corresponding author. Email: aaron.wheeler@utoronto.ca

Published 15 July 2020, *Sci. Adv.* **6**, eaba9589 (2020)
DOI: 10.1126/sciadv.aba9589

This PDF file includes:

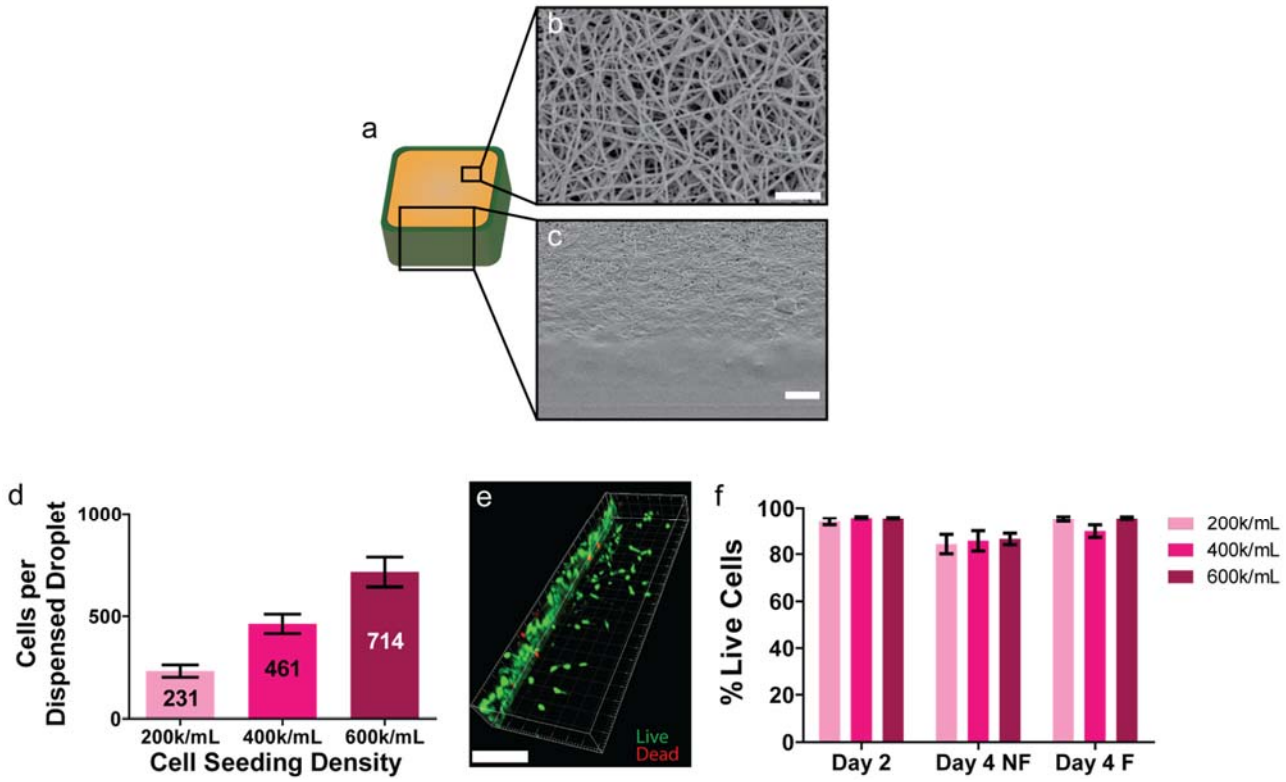

Supplementary Figure S1 CIMMS microgels and cell viability. For (a-c) core-shell microgels were formed from 2.4 mg/mL collagen I and 10% BM extract. (a) Cartoon indicating the orientation of the microgel shown in the images. SEM images of (b) the collagen I core (scale bar = 20 μm) and (c) the edge of microgel with core on the "top" and the shell on the "bottom" (scale bar = 100 μm). The pore size of the collagen I core was calculated to be 3.1 μm by the method reported by Blackmon et al. (*53*), which is nearly identical to the pore size reported for the same concentration of collagen I cast in well plates by Lang et al. (*54*). For (d-f) MDA-MB-231 cells were seeded onto simple collagen I microgels (2.4 mg/mL). (d) Cell count per droplet with seeding density at 200,000 (lt. pink), 400,000 (fuscia) or 600,000 cells/mL (burgundy). Error bars represent ± 1 std. dev. from $n = 4$ microgels per condition. (e) 3D confocal fluorescent microscopy image of cells stained on day 4 with calcein-AM (live-green) and propidium iodide (dead-red). Scale bar = 200 μm. (f) Percentages of live cells seeded at different densities in CIMMS devices and cultured to day 2, day 4 with no "feed" (media supplement) (NF), and day 4 after feeding on day 2 (F). Error bars represent ± 1 std. dev. from $n = 6$-12 microgels per condition.

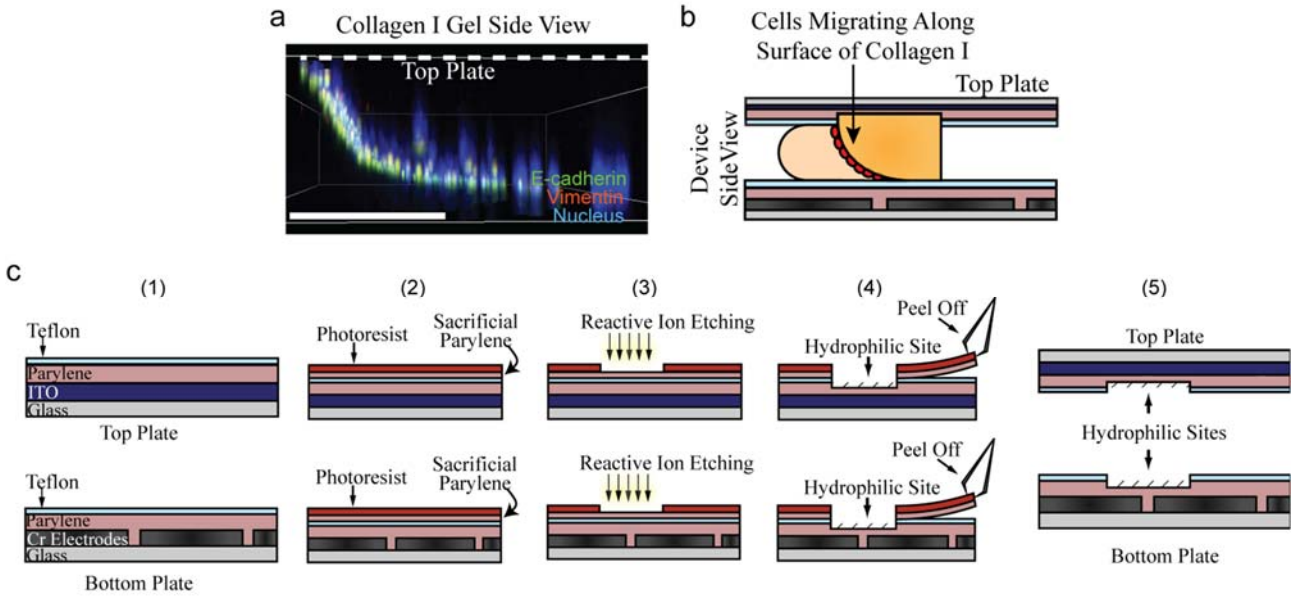

Supplementary Figure S2 CIMMS device optimization. (a-b) Method reported previously [Eydelnant et al. (*17*), not used in most experiments here] for forming microgels anchored asymmetrically on only the DMF top plate. (a) 3D confocal image of a side view of a simple collagen I microgel (2.4 mg/mL) formed using the Eydelnant et al. technique. The image was collected on day 4 after seeding with MDA-MB-231 cells at 50,000 cells/mL and immunostaining for nucleus–blue, E-cadherin—green, and vimentin—red. The dashed line indicates the surface of the top plate. Scale bar = 200 μm. (b) Cartoon rendering of the conditions in (a), with hydrophilic anchor only on the top plate (and not on the bottom). (c) Cartoon illustrating the new process introduced here for forming symmetric pairs of hydrophilic spots on top and bottom plates of CIMMS devices, overcoming the limitations of the Eydelnant et al. technique. (1) Top plate bearing continuous ITO electrode (dark blue) (top) and bottom plate bearing patterned chromium electrodes (black) (bottom), coated with parylene-C (salmon) and Teflon AF (light blue). (2) A layer of sacrificial parylene-C (~1 μm) is deposited on top of DMF top and bottom plates, followed by spin-coating with photoresist (burgundy). (3) The photoresist is photopatterned, followed by reactive ion etching (RIE). (4) After RIE, the residual sacrificial layer is peeled off. (5) The resulting top and bottom plates are aligned and affixed with matching, symmetric pairs of hydrophilic spots.

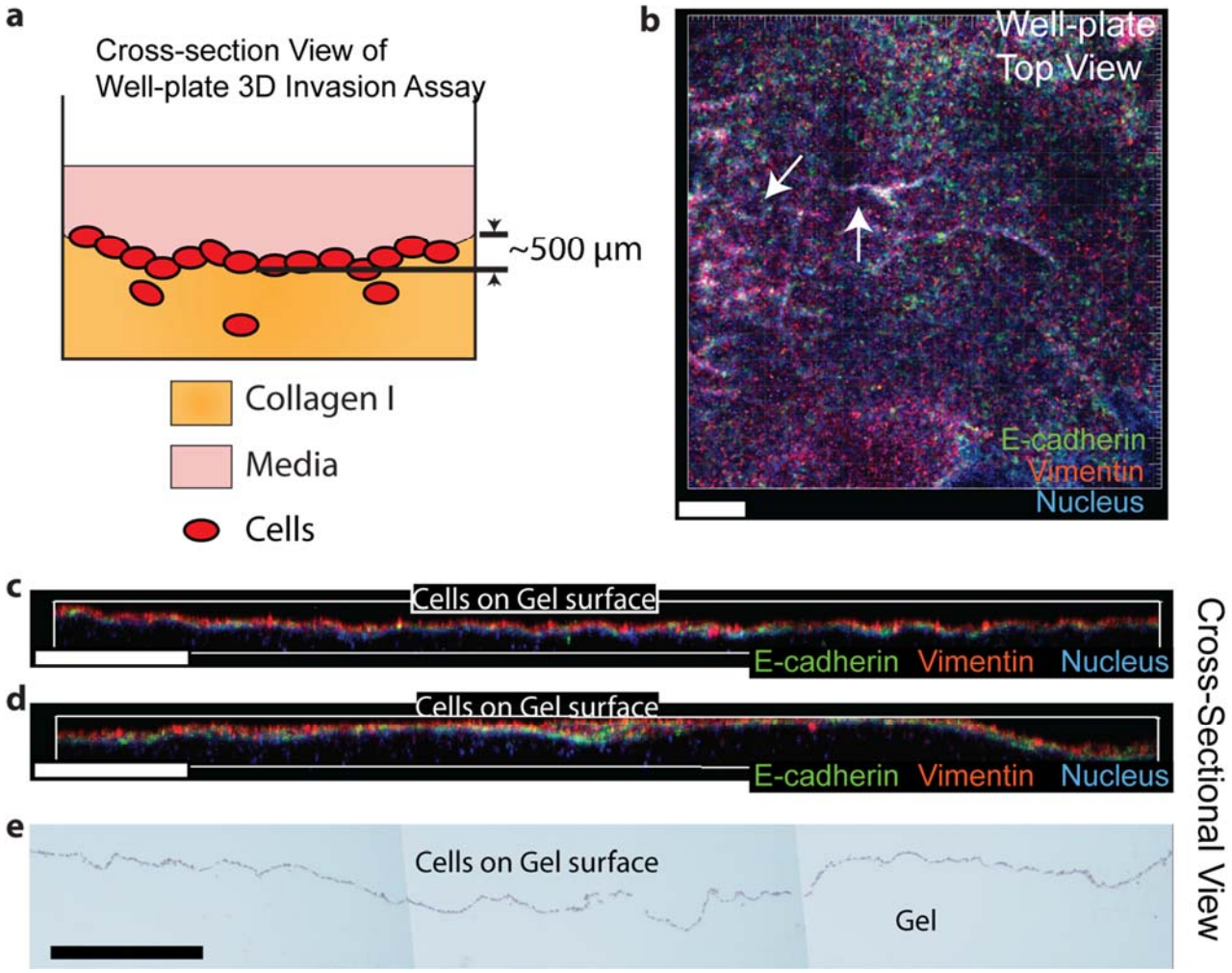

Supplementary Figure S3 Well-plate vertical gel invasion assays. (a) Cross-section cartoon of a vertical well-plate gel invasion assay. (b) Stitched top-view of confocal 3D image of MDA-MB-231 cells on the surface of a collagen I microgel in a well-plate. White arrows indicate ripples on gel surface. (c, d) Cross-sectional images from the microgel in (b) showing uneven gel surface. (e) Stitched bright-field microscopy image of cryosectioned collagen I gel with MDA-MB-231 cells showing cells on uneven surface. Scale bar b-e = 500 µm. For all images in this figure, cells were seeded at 100,000/mL onto simple collagen I microgels in well plates (2.4 mg/mL) and cultured to day 4, and in immunofluorescence images, cells were stained for E-cadherin (green), vimentin (red), and nucleus (blue).

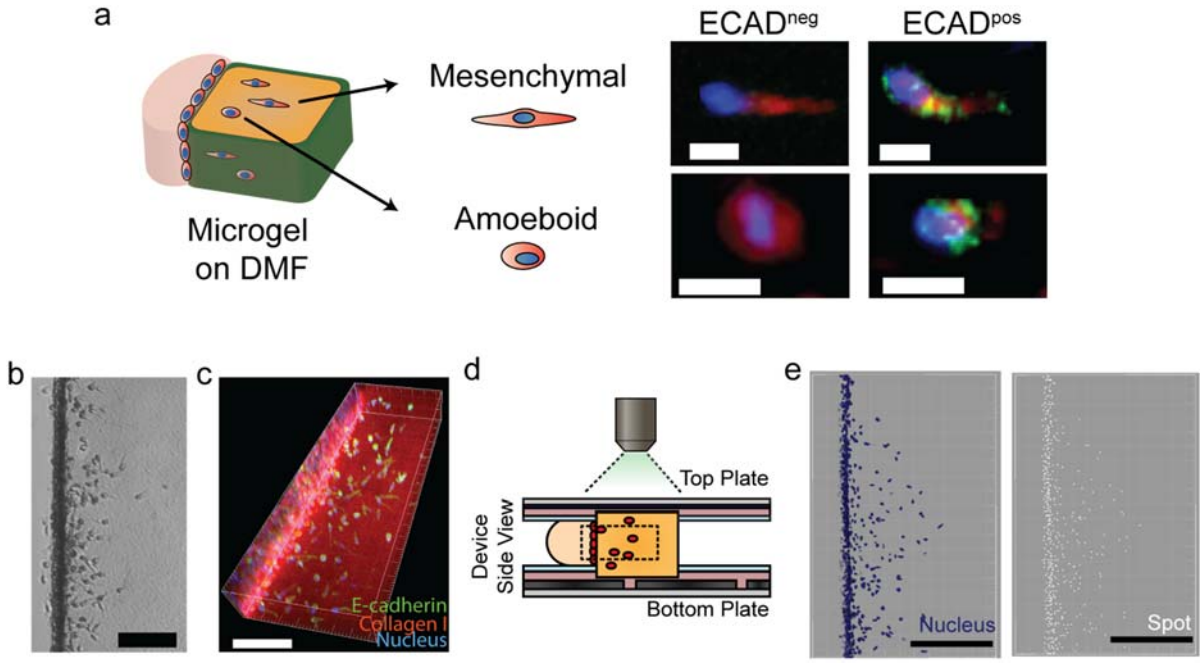

Supplementary Figure S4 Advantages of CIMMS. (a) High-resolution confocal microscopy in CIMMS allows visualization of invading cell morphology. Cartoon of cells invading into a core-shell microgel (left) highlighting mesenchymal and amoeboid morphology, and confocal 3D images (right) of 4 different cells, each with different combination of morphology (mesenchymal-top vs. amoeboid-bottom) and E-cadherin expression (negative: $ECAD^{neg}$, left; positive: $ECAD^{pos}$, right) negative-left). MD-MBA-231 cells shown here (seeded at 400,000/mL, cultured to day 4) have invaded into core-shell microgels formed from 2.4 mg/mL collagen I and 10% BM extract. Cells were stained for E-cadherin (green), vimentin (red), and nucleus (blue). Scale bars = 20 μm. (b-c) CIMMS microgels do not experience surface rippling. (b) Bright-field microscopy image of MDA-MB-231 cells invading into a simple collagen I microgel (2.4 mg/mL), 4 days after seeding at 400,000/mL. (c) Confocal 3D microscopy image of the same gel stained for nucleus (blue), collagen I (red), and E-cadherin (green). The collagen I staining shows a straight microgel edge. (b, c) Scale bars = 200 μm. (d, e) Automated quantification of invading cells in CIMMS. (d) Side-view cartoon of CIMMS device illustrating the imaging setup. The dotted black rectangle indicates the section of the microgel used for quantification studies; cells outside of this section are ignored. (e) Processed confocal images of MDA-MB-231 cells invading into a simple collagen I microgel (2.4 mg/mL) 4 days after seeding at 400,000/mL. Locations of cells are automatically tracked and indicated by nuclei (blue) as shown in the left panel. A custom script running in IMARIS 3D image analysis software identifies the 3D coordinates of nuclei in white spots (right panel). Scale bar = 150 μm.

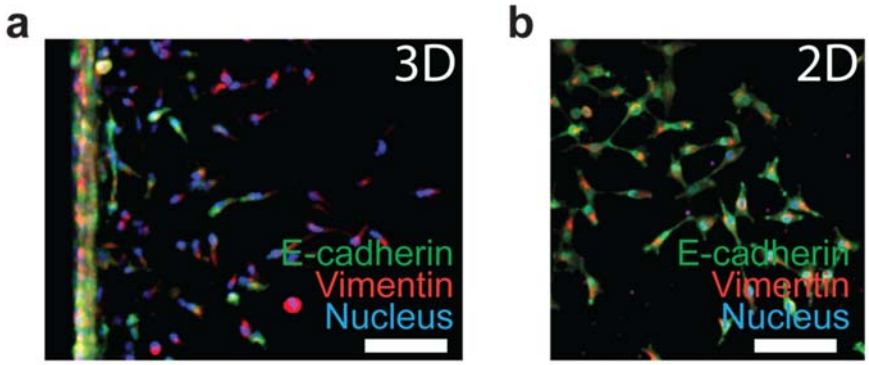

Supplementary Figure S5 Invading cell heterogeneity. (a) Top view of confocal 3D image of MDA-MB-231 cells, day 4 after seeding at 400,000/mL on a simple microgel formed from 2.4 mg/mL collagen I in a CIMMS device. (b) Confocal 2D image of MDA-MB-231 cells on day 4 after seeding at 50,000/mL on 8-well chamber slides. In both images, cells are immunofluorescently labeled for E-cadherin (green), vimentin (red), nucleus (blue), and the scale bar = 100 μm.

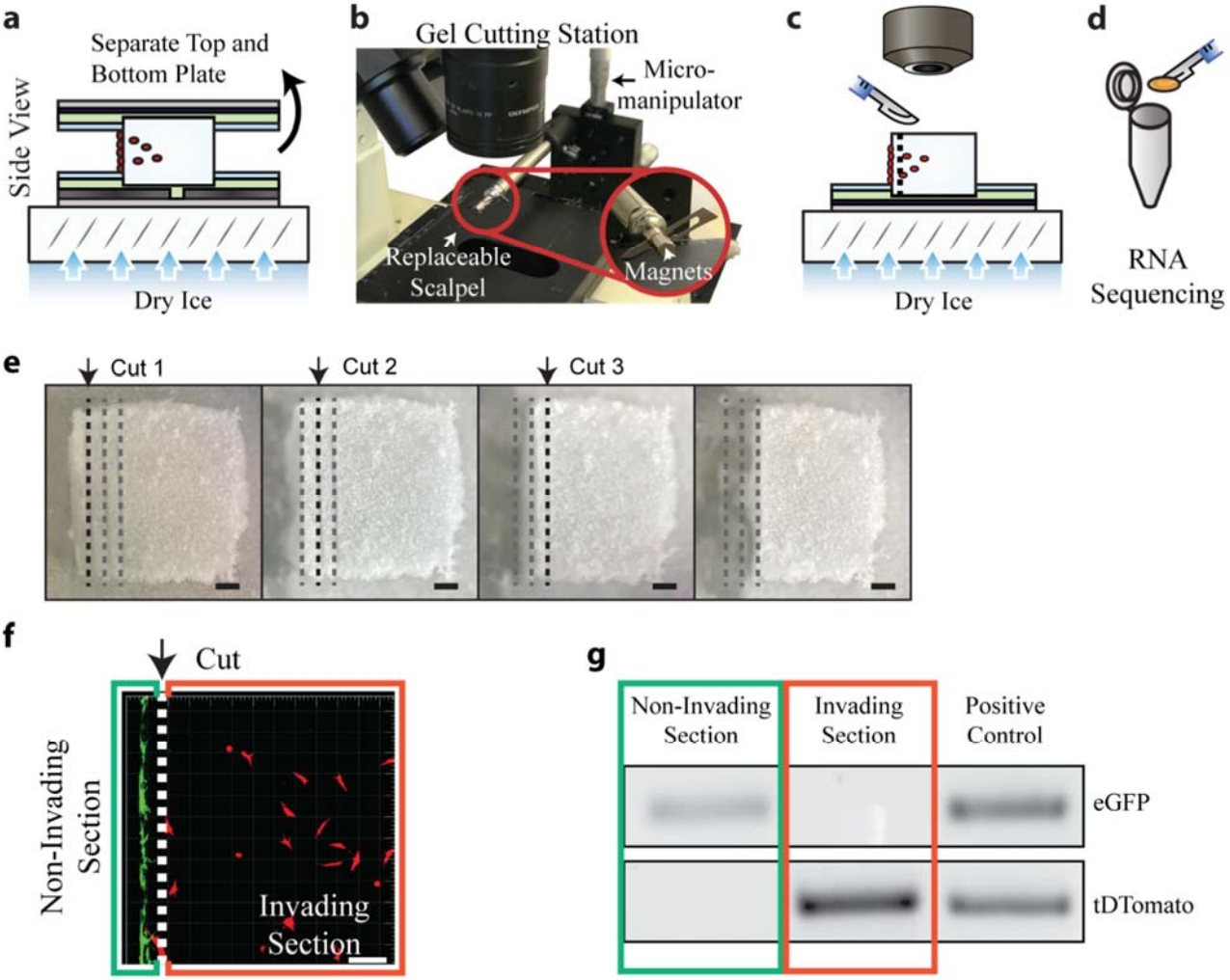

Supplementary Figure S6 Microgel dissection for analysis of transcriptomes of invading cells in CIMMS. (a) Cartoon illustrating the process of freeze-drying microgels *in situ* on an aluminum plate chilled with dry ice. (b,c) Picture and cartoon of the custom dissection station (featuring replaceable scalpels affixed magnetically onto a 3-axis micromanipulator) used to process microgels with invading cells. (d) Cartoon illustrating how microgel slices were collected and evaluated for gene transcripts. (e) Pictures of a simple collagen I microgel (2.4 mg/mL) being dissected into ~100 µm thick slices. Scale bar = 150 µm. (f) Top-view of a 3D confocal microscopy image of a simple collagen I microgel (2.4 mg/mL) used for a pseudo-invasion assay with tDTomato-expressing B16 cells pre-mixed in the collagen prior to gelling to mimic "invading" cells, and eGFP-expressing U87 cells seeded on the edge of the gel to represent "non-invading" cells. Scale bar = 150 µm. (g) Representative pictures of agarose gels from a pseudo-invasion assay featuring bands for transcripts of eGFP (top) and tDTomato (bottom) for the dissected slices of "non-invading" (left, outlined in green) and "invading" (middle, outlined in red) cells, and a positive control for both transcripts (right). Forward (fwd) and reverse (rev) primers were fwd-eGFP: 5'-GAAGCAGCAGCACTTCTTCAA-3', rev-eGFP: 5'-AAGTCGATGCCCTTCAGCTC-3', fwd-tDTomato: 5'-AGCAAGGGCGAGGAGGTCATC-3' , and rev-tDTomato: 5'-CCTTGGAGCCGTACATGAACTGG-3'. Photo credits: B.B. Li, Univ. Toronto.

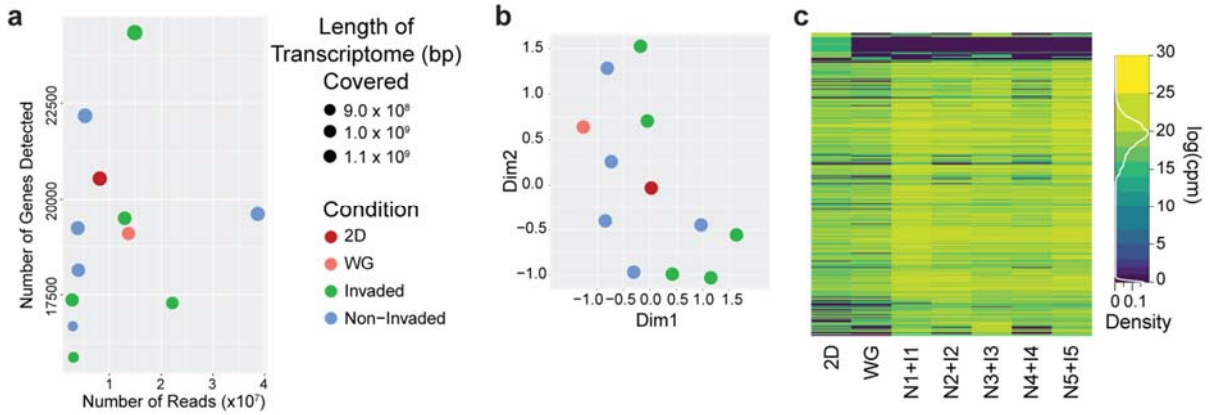

Supplementary Figure S7 Performance characterization of CIMMS samples and controls evaluated by RNA-seq. The samples include five invaded (I1-5) and non-invaded (N1-5) sub-populations of MDA-MB-231 cells harvested from dissections of simple collagen I microgels (2.4 mg/mL) on day 4 after seeding at 400,000 cells/mL in CIMMS experiments, a whole-gel control (WG) from an identical CIMMS experiment with no dissection, and a two-dimensional culture control (2D) from identical conditions (but with no hydrogel, invasion, or dissection) in a well-plate. (a) Numbers of genes detected as a function of the numbers of reads per sample for the invaded samples (green), the non-invaded samples (blue), the WG control (orange), and the 2D control (red). The length of the transcriptome (in bp) is represented by marker size. (b) Plot representing dimensional reduction (to Dim1 and Dim2) of all sample-data by UMAP (*50*) with the same legend from panel a. (c) Heat map of gene expression level [shown as the base-10 logarithm of counts per million (CPM), where yellow = high and blue = low] of the 454 genes (rows) with expression-level differences of $p < 0.01$ (based upon a quasi-likelihood negative binomial generalized log-linear model, glmQLFit, from edgeR (*51*) for seven samples (columns) including 2D and WG controls, and pooled expression from pairs of invaded and non-invaded cells (i.e., I1+N1, I2+N2, I3+N3, I4+N4, and I5+N5). The white trace labeled "density" in the legend represents the distribution of the different expression levels in the data-set.

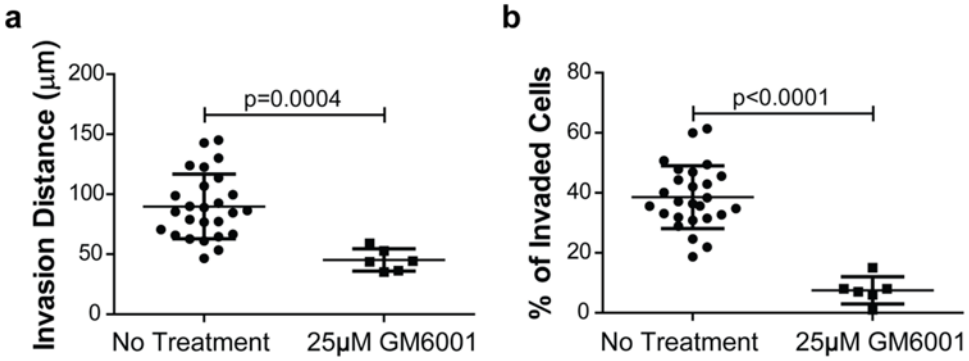

Supplementary Figure S8 Effect of ilomastat (GM6001) on invasion of MDA-MB-231 cells. Invasion distance (a) and % of invaded cells (b) for MDA-MB-231 cells seeded at 400,000/mL on simple microgels (formed from 2.4 mg/mL collagen I) and cultured to day 4 with (squares) and without (circles) exposure to 25 µM GM6001. Error bars represent ±1 std. deviation for $n > 6$ microgels per condition.

Supplementary Table S1

Table S1, List 1. 244 genes identified by differential gene analysis (comparing invading and non-invading cells in CIMMS experiments), from heat-map in Fig. 5a in the main text.			
Gene Stable ID	**Gene Name**	**logFoldChange**	**FDR**
ENSG00000069399.14	BCL3	3.741800615	0.004834
ENSG00000019582.14	CD74	5.265939536	0.00085
ENSG00000105289.14	TJP3	5.086877438	0.009076
ENSG00000106541.11	AGR2	6.9108305	0.002075
ENSG00000110492.15	MDK	3.244112905	0.028835
ENSG00000127561.14	SYNGR3	8.938689005	0.003358
ENSG00000138131.3	LOXL4	6.19674347	0.000239
ENSG00000152128.13	TMEM163	8.666358509	5.85E-05
ENSG00000158828.7	PINK1	2.920168609	0.032696
ENSG00000166592.11	RRAD	5.647772761	0.001211
ENSG00000169583.12	CLIC3	6.127603687	0.000579
ENSG00000170577.7	SIX2	7.349364463	0.000425
ENSG00000233384.2	AC096537.1	10.76800333	0.000199
ENSG00000006210.6	CX3CL1	10.77834873	0.000244
ENSG00000005243.9	COPZ2	6.802951259	0.00085
ENSG00000012171.19	SEMA3B	4.451958057	0.002215
ENSG00000012779.10	ALOX5	5.057244647	0.039191
ENSG00000025708.13	TYMP	7.333335447	0.000185
ENSG00000028137.18	TNFRSF1B	11.73664133	0.000143
ENSG00000039068.18	CDH1	9.024095046	0.003352
ENSG00000064300.8	NGFR	9.79289492	0.0009
ENSG00000064886.13	CHI3L2	5.121509204	0.002712
ENSG00000070404.9	FSTL3	3.616068286	0.012989
ENSG00000074410.13	CA12	4.1646515	0.005667
ENSG00000077984.5	CST7	4.273949165	0.03687
ENSG00000082781.11	ITGB5	3.358444798	0.011214
ENSG00000088280.18	ASAP3	3.636498118	0.011289
ENSG00000090238.11	YPEL3	2.977074276	0.028426
ENSG00000090376.10	IRAK3	3.590521154	0.032589
ENSG00000092621.11	PHGDH	8.075634701	0.027661
ENSG00000100031.18	GGT1	3.524565515	0.028107
ENSG00000100234.11	TIMP3	3.603893105	0.02982
ENSG00000100290.2	BIK	7.317375477	0.000237
ENSG00000101439.8	CST3	4.152288429	0.023457
ENSG00000101460.12	MAP1LC3A	6.644031488	0.00093
ENSG00000103490.13	PYCARD	9.106165156	0.004201
ENSG00000104368.17	PLAT	3.07908136	0.03077
ENSG00000104870.12	FCGRT	4.839756422	0.002504

Table S1, List 1. 244 genes identified by differential gene analysis (comparing invading and non-invading cells in CIMMS experiments), from heat-map in Fig. 5a in the main text.

Gene Stable ID	Gene Name	logFoldChange	FDR
ENSG00000105699.16	LSR	3.139865058	0.02604
ENSG00000106003.12	LFNG	5.823873698	0.008113
ENSG00000106078.17	COBL	8.047431092	0.016154
ENSG00000106123.11	EPHB6	8.248692046	0.014373
ENSG00000108551.4	RASD1	4.503832014	0.008113
ENSG00000109321.10	AREG	3.947161565	0.009899
ENSG00000109472.13	CPE	3.827167021	0.008265
ENSG00000109610.5	SOD3	3.585626958	0.014299
ENSG00000111319.12	SCNN1A	4.359374186	0.010955
ENSG00000113083.13	LOX	3.642093925	0.010094
ENSG00000117983.17	MUC5B	9.096762277	0.00395
ENSG00000121858.10	TNFSF10	6.981679796	0.011289
ENSG00000122711.8	SPINK4	9.676938269	0.004848
ENSG00000123095.5	BHLHE41	3.062744239	0.02604
ENSG00000124664.10	SPDEF	6.684650755	0.002075
ENSG00000125730.16	C3	5.881624042	0.000799
ENSG00000127324.8	TSPAN8	8.948892732	0.000667
ENSG00000130513.6	GDF15	5.36825719	0.001718
ENSG00000132821.11	VSTM2L	6.752933332	0.001777
ENSG00000134184.12	GSTM1	3.842963751	0.025544
ENSG00000135929.8	CYP27A1	3.054049486	0.044442
ENSG00000140937.13	CDH11	3.002938124	0.022229
ENSG00000141040.14	ZNF287	7.778815617	0.032589
ENSG00000143365.17	RORC	8.363679811	0.010415
ENSG00000146678.9	IGFBP1	2.938744554	0.045712
ENSG00000147676.13	MAL2	10.71252644	5.85E-05
ENSG00000151468.10	CCDC3	6.085876305	0.00451
ENSG00000156453.13	PCDH1	8.894600512	0.005452
ENSG00000157303.10	SUSD3	12.60765399	5.85E-05
ENSG00000158050.4	DUSP2	9.576800072	0.002121
ENSG00000160182.2	TFF1	8.910554694	0.013837
ENSG00000160223.16	ICOSLG	5.377057011	0.013032
ENSG00000161798.6	AQP5	7.882867608	0.028718
ENSG00000162576.16	MXRA8	11.14227622	8.25E-05
ENSG00000162777.16	DENND2D	7.7703824	0.001342
ENSG00000163694.14	RBM47	4.066220789	0.025379
ENSG00000163739.4	CXCL1	3.134986198	0.032589
ENSG00000163864.15	NMNAT3	8.321656646	0.010559
ENSG00000163874.10	ZC3H12A	3.69777341	0.004699

Table S1, List 1. 244 genes identified by differential gene analysis (comparing invading and non-invading cells in CIMMS experiments), from heat-map in Fig. 5a in the main text.

Gene Stable ID	Gene Name	logFoldChange	FDR
ENSG00000163993.6	S100P	4.822344813	0.011408
ENSG00000164442.9	CITED2	3.306061996	0.017142
ENSG00000165272.14	AQP3	5.492699314	0.012165
ENSG00000165949.12	IFI27	4.401590457	0.014048
ENSG00000166126.10	AMN	8.394815873	0.014265
ENSG00000166510.13	CCDC68	2.824129116	0.038801
ENSG00000166920.12	C15orf48	3.354661222	0.016287
ENSG00000167191.11	GPRC5B	9.590551843	0.000882
ENSG00000167536.13	DHRS13	3.03316683	0.032589
ENSG00000168140.4	VASN	7.461815174	0.000224
ENSG00000168528.11	SERINC2	5.130714247	0.000667
ENSG00000170542.5	SERPINB9	9.022237192	0.000199
ENSG00000171345.13	KRT19	7.630231461	0.00036
ENSG00000172201.11	ID4	5.335591157	0.011408
ENSG00000173156.6	RHOD	11.74092331	5.85E-05
ENSG00000173432.10	SAA1	7.81849889	0.000185
ENSG00000173918.14	C1QTNF1	6.210468593	0.015658
ENSG00000174080.10	CTSF	7.073500115	0.00036
ENSG00000175591.11	P2RY2	4.884686288	0.027325
ENSG00000177096.8	PHETA2	9.169028349	0.002504
ENSG00000177191.2	B3GNT8	7.315384879	0.00395
ENSG00000182809.10	CRIP2	5.237411511	0.000807
ENSG00000183914.14	DNAH2	5.601789118	0.004848
ENSG00000184371.13	CSF1	5.380216772	0.001194
ENSG00000184454.6	NCMAP	8.181839676	0.014638
ENSG00000184985.16	SORCS2	10.40690914	0.000491
ENSG00000185585.19	OLFML2A	4.009428454	0.024748
ENSG00000196154.11	S100A4	7.242590237	0.000418
ENSG00000196664.4	TLR7	7.704610698	0.043869
ENSG00000197253.13	TPSB2	7.989424683	0.024706
ENSG00000197766.7	CFD	3.503337622	0.014265
ENSG00000221869.4	CEBPD	3.760183323	0.013837
ENSG00000233338.1	TLR8-AS1	6.851140951	0.026448
ENSG00000240859.1	AC093627.10	7.92532393	0.016287
ENSG00000243649.8	CFB	8.682823058	0.00029
ENSG00000244731.7	C4A	4.348862096	0.029964
ENSG00000264230.7	ANXA8L1	5.175025552	0.002868
ENSG00000275395.4	FCGBP	4.672133875	0.035087
ENSG00000275896.5	PRSS2	11.35858866	0.000147

Table S1, List 1. 244 genes identified by differential gene analysis (comparing invading and non-invading cells in CIMMS experiments), from heat-map in Fig. 5a in the main text.

Gene Stable ID	Gene Name	logFoldChange	FDR
ENSG00000276850.4	AC245041.2	5.487523211	0.004966
ENSG00000277117.4	FP565260.3	5.467204345	0.018128
ENSG00000101441.4	CST4	8.79382523	0.000184
ENSG00000090339.8	ICAM1	3.08641955	0.032589
ENSG00000116661.9	FBXO2	11.99437893	0.000129
ENSG00000124107.5	SLPI	4.068635045	0.012542
ENSG00000125731.12	SH2D3A	4.85214036	0.012411
ENSG00000152137.6	HSPB8	8.132067822	0.020521
ENSG00000154930.14	ACSS1	3.647900578	0.025068
ENSG00000170412.16	GPRC5C	9.321747354	0.00196
ENSG00000184292.6	TACSTD2	2.997959989	0.031765
ENSG00000185338.4	SOCS1	5.771044472	0.000496
ENSG00000188820.12	CALHM6	10.06699633	0.001211
ENSG00000253958.1	CLDN23	3.364750665	0.028181
ENSG00000266865.6	AC138207.8	3.972896128	0.045712
ENSG00000273415.1	AP000904.1	6.723448005	0.015658
ENSG00000103888.16	CEMIP	7.855585193	0.00036
ENSG00000099998.17	GGT5	5.559290753	0.000697
ENSG00000105204.13	DYRK1B	4.525327582	0.025519
ENSG00000106538.9	RARRES2	12.07058209	0.000147
ENSG00000117122.13	MFAP2	2.855583286	0.030071
ENSG00000128422.15	KRT17	5.182086699	0.022023
ENSG00000136732.14	GYPC	9.069318861	0.004812
ENSG00000141753.6	IGFBP4	5.632797589	0.004938
ENSG00000171227.6	TMEM37	3.219027022	0.024748
ENSG00000271447.5	MMP28	8.5929242	0.009798
ENSG00000085831.15	TTC39A	4.18114176	0.043158
ENSG00000069482.6	GAL	10.7758457	0.00036
ENSG00000102109.8	PCSK1N	10.68026347	0.000378
ENSG00000108387.14	SEPTIN4	5.648583191	0.001532
ENSG00000109943.8	CRTAM	8.224303025	0.021141
ENSG00000134339.8	SAA2	10.01963819	5.85E-05
ENSG00000136542.8	GALNT5	10.07402688	0.000807
ENSG00000148346.11	LCN2	14.15599939	8.25E-05
ENSG00000164530.13	PI16	11.30963891	0.000185
ENSG00000167157.10	PRRX2	7.537026039	0.04739
ENSG00000184012.11	TMPRSS2	8.335037882	0.012542
ENSG00000198223.16	CSF2RA	5.998392177	0.00329
ENSG00000198223.16_PAR_Y	ENSG00000198223.16_PAR_Y	5.998392177	0.00329

Table S1, List 1. 244 genes identified by differential gene analysis (comparing invading and non-invading cells in CIMMS experiments), from heat-map in Fig. 5a in the main text.

Gene Stable ID	Gene Name	logFoldChange	FDR
ENSG00000213626.11	LBH	5.810555384	0.020938
ENSG00000102934.9	PLLP	6.920625199	0.000129
ENSG00000095303.14	PTGS1	8.395475706	0.020628
ENSG00000115226.9	FNDC4	7.953899963	0.000418
ENSG00000115919.14	KYNU	3.886586392	0.021141
ENSG00000131746.12	TNS4	7.524739125	0.037927
ENSG00000146674.14	IGFBP3	4.372242469	0.004834
ENSG00000162174.12	ASRGL1	7.732020422	0.04035
ENSG00000265190.6	ANXA8	6.335848901	0.000875
ENSG00000166741.7	NNMT	3.203909001	0.02982
ENSG00000164855.15	TMEM184A	8.773941849	0.00395
ENSG00000182326.14	C1S	3.94036669	0.022184
ENSG00000168874.12	ATOH8	4.833456135	0.03823
ENSG00000129757.12	CDKN1C	4.556358011	0.001718
ENSG00000173801.16	JUP	2.836640723	0.030448
ENSG00000142765.17	SYTL1	3.722787447	0.041075
ENSG00000115468.11	EFHD1	4.7038203	0.035432
ENSG00000166145.14	SPINT1	9.753124403	0.000135
ENSG00000175130.6	MARCKSL1	3.134602716	0.033057
ENSG00000197927.12	C2orf27A	8.173270642	0.020122
ENSG00000109072.13	VTN	7.772188931	0.027584
ENSG00000104892.16	KLC3	5.703807945	0.011143
ENSG00000162383.11	SLC1A7	7.624674934	0.045976
ENSG00000164761.8	TNFRSF11B	2.982728335	0.035561
ENSG00000165474.5	GJB2	4.658004582	0.00329
ENSG00000203805.10	PLPP4	4.485747557	0.00329
ENSG00000215182.8	MUC5AC	9.001841888	0.003352
ENSG00000176046.8	NUPR1	4.937920291	0.020122
ENSG00000159403.15	TFF3	3.747057619	0.006557
ENSG00000114631.10	PODXL2	4.964227688	0.004303
ENSG00000163435.15	ELF3	7.943730245	0.014299
ENSG00000179403.11	VWA1	6.044392991	0.000437
ENSG00000170369.3	CST2	5.201978696	0.00329
ENSG00000163814.7	CDCP1	4.285694169	0.003352
ENSG00000115380.19	EFEMP1	5.900277521	0.000491
ENSG00000104140.6	RHOV	10.40532107	0.000143
ENSG00000167703.14	SLC43A2	4.10944022	0.005963
ENSG00000168487.17	BMP1	3.285589705	0.023245
ENSG00000248890.1	HHIP-AS1	5.009861023	0.008265

Table S1, List 1. 244 genes identified by differential gene analysis (comparing invading and non-invading cells in CIMMS experiments), from heat-map in Fig. 5a in the main text.

Gene Stable ID	Gene Name	logFoldChange	FDR
ENSG00000154262.12	ABCA6	5.921044322	0.025684
ENSG00000132879.13	FBXO44	4.327858399	0.024248
ENSG00000159167.11	STC1	9.551004417	0.000101
ENSG00000175274.18	TP53I11	10.20414493	0.000697
ENSG00000117984.13	CTSD	5.035733496	0.002783
ENSG00000113504.20	SLC12A7	8.995120159	0.004692
ENSG00000137699.16	TRIM29	9.084286443	0.011214
ENSG00000165716.10	FAM69B	5.064908439	0.02353
ENSG00000224389.8	C4B	4.500603214	0.026563
ENSG00000187017.15	ESPN	8.051130781	0.016782
ENSG00000170442.11	KRT86	3.120480286	0.033794
ENSG00000235098.8	ANKRD65	4.472546723	0.045976
ENSG00000136859.9	ANGPTL2	11.79982587	5.85E-05
ENSG00000129988.5	LBP	8.386063264	0.012677
ENSG00000176485.11	PLA2G16	2.957298947	0.045712
ENSG00000215845.10	TSTD1	6.678862044	0.000882
ENSG00000167772.11	ANGPTL4	3.044899098	0.044442
ENSG00000162366.7	PDZK1IP1	12.44568748	0.000147
ENSG00000172236.16	TPSAB1	7.96551086	0.025519
ENSG00000188002.10	AC026412.1	4.402807704	0.002401
ENSG00000150556.16	LYPD6B	8.994082272	0.002984
ENSG00000107738.19	VSIR	3.983357181	0.019779
ENSG00000164488.11	DACT2	8.607251915	0.009661
ENSG00000137880.5	GCHFR	6.562541616	0.00467
ENSG00000135480.15	KRT7	3.642926309	0.020521
ENSG00000160180.15	TFF3	10.36917545	0.00094
ENSG00000232774.7	FLJ22447	6.036131704	0.003787
ENSG00000189143.9	CLDN4	7.238677628	0.000486
ENSG00000169026.12	SLC49A3	4.241838359	0.016254
ENSG00000187566.5	NHLRC1	9.210315145	0.00243
ENSG00000205809.9	KLRC2	3.598543353	0.021722
ENSG00000177989.13	ODF3B	4.796273791	0.002075
ENSG00000175315.2	CST6	9.038439197	0.000127
ENSG00000171051.8	FPR1	6.946906921	0.008113
ENSG00000261371.5	PECAM1	6.255278357	0.002107
ENSG00000211445.11	GPX3	6.264053033	0.00036
ENSG00000126759.13	CFP	5.146941361	0.002783
ENSG00000119630.13	PGF	3.843993595	0.00539
ENSG00000237594.2	AP000251.1	7.587326248	0.048546

Table S1, List 1. 244 genes identified by differential gene analysis (comparing invading and non-invading cells in CIMMS experiments), from heat-map in Fig. 5a in the main text.

Gene Stable ID	Gene Name	logFoldChange	FDR
ENSG00000179862.6	CITED4	4.955169609	0.013582
ENSG00000130203.9	APOE	5.687432074	0.000936
ENSG00000186496.10	ZNF396	7.528551338	0.032589
ENSG00000170373.8	CST1	7.898112488	0.000667
ENSG00000189350.12	TOGARAM2	6.050262364	0.015038
ENSG00000174307.6	PHLDA3	3.855160812	0.006886
ENSG00000182871.14	COL18A1	3.609183795	0.009899
ENSG00000171631.14	P2RY6	8.151292837	0.009661
ENSG00000166033.11	HTRA1	3.158098503	0.025544
ENSG00000182272.11	B4GALNT4	9.192758787	0.003352
ENSG00000160181.8	TFF2	9.666305469	0.00395

Table S1, List 2. Pathways and gene ontologies enriched ($p < 0.05$) from differentially expressed genes in Table S1, List 1, determined using gene ontologies (GO) and WikiPathways 2019 (WP) derived from EnrichR.

Term	Adjusted p-value*
Pathway	
Complement Activation WP545	2.47E-06
Selenium Micronutrient Network WP15	2.17E-05
Human Complement System WP2806	4.42E-04
Folate Metabolism WP176	0.001432005
Vitamin D Receptor Pathway WP2877	0.001728055
Vitamin B12 Metabolism WP1533	0.002417028
Complement and Coagulation Cascades WP558	0.004866447
Glutathione metabolism WP100	0.009261168
Gene Ontology: Biological Process	
regulation of cysteine-type endopeptidase activity (GO:2000116)	6.15E-05
negative regulation of endopeptidase activity (GO:0010951)	1.87E-04
negative regulation of cysteine-type endopeptidase activity (GO:2000117)	0.004899642
extracellular matrix organization (GO:0030198)	0.006492703
response to molecule of bacterial origin (GO:0002237)	0.028553518
cellular response to cytokine stimulus (GO:0071345)	0.040090517
proteolysis (GO:0006508)	0.040126753
positive regulation of apoptotic cell clearance (GO:2000427)	0.043600872
cytokine-mediated signaling pathway (GO:0019221)	0.047057545
cellular protein metabolic process (GO:0044267)	0.04978941
Gene Ontology: Molecular Function	
endopeptidase inhibitor activity (GO:0004866)	4.28E-04
serine-type endopeptidase activity (GO:0004252)	5.25E-04

Table S1, List 2. Pathways and gene ontologies enriched ($p < 0.05$) from differentially expressed genes in Table S1, List 1, determined using gene ontologies (GO) and WikiPathways 2019 (WP) derived from EnrichR.	
Term	**Adjusted p-value***
protease binding (GO:0002020)	5.60E-04
serine-type peptidase activity (GO:0008236)	6.51E-04
cysteine-type endopeptidase inhibitor activity (GO:0004869)	6.93E-04
endopeptidase activity (GO:0004175)	0.006051649
insulin-like growth factor II binding (GO:0031995)	0.008605042
omega peptidase activity (GO:0008242)	0.009834333

* The adjusted p-value is computed in EnrichR from the Fisher exact test (*28*).

Supplementary Table S2.

Table S2, List 1. Genes identified from CIMMS experiments associated with invasive phenotype from WGCNA gene module MEdarkseagreen4 from Fig. 6c in the main text.
OVGP1, VSX1, AURKC, HYAL4, CLEC2B, MGP, CNR1, UNC13A, CHRM3, KLRC1, FHDC1, DNAJA4, ARMC12, CXCL1, LINC01600, P2RY6, RCAN2, DPY19L2, KPNA7, AMY1C, IGFL4, LINC01460, KLRC3, RNU6-9, FTH1P3, SULT1A4, LINC02649, AL031777.1, FTH1P8, OSTCP4, FTH1P10, AC093107.1, AL663058.1, AC064875.1, PSPC1-AS2, AL158166.1, FTH1P16, LTB, AL121987.2, LINC01693, CALM2P2, AL450322.2, FTH1P5, CCDC192, AL356583.3, RPL31P2, LINC02015, AL671986.1, FTH1P1, AC002480.1, HMGN2P35, EIF4EP1, GAS6-AS1, LINC01505, BX005266.3, FTH1P2, AC068580.3, BX284668.4, LINC00957, MRPS10P1, FTH1P11, TNFRSF14-AS1, AL354989.2, FTH1P23, CFAP57, WWP1P1, AP003733.1, AC096577.1, KRT8P46, AC034213.1, SNHG27, AC083973.1, AC022868.1, NAP1L1P1, ATP5PBP5, AC136475.3, AC109635.4, AP003062.1, AL583722.1, AC025154.2, MTCO1P2, AC110588.1, CRTC3-AS1, AP003469.4, AC026471.4, AC103988.1, Z92544.2, TVP23CP2, AC005779.1, AC007842.1, AC010487.2, PHBP20, AL158801.4, AL137003.2, AC116036.2, AL357054.4, AC104964.4, AC027271.1, AP001437.1, AL136295.6, AC131009.4, AC093525.9, AC073548.1, AC005355.2

Table S2, List 2. Genes identified from CIMMS experiments associated with invasive phenotype from WGCNA gene module MEindianred4 from Fig. 6c in the main text.
SHF, PPIAP72, ZNF154, RNVU1-3, EEF1A1P16, AL513523.1, DSTNP1, AL353596.1, AL024508.1, CDC42P1, AL163973.1, OR7E53P, RPS27P21, RPL31P61, RPL26P35, CR545473.1, PRELID1P4, AC010168.2, AC013468.1, AC108673.3

Table S2, List 3. Genes identified from CIMMS experiments associated with non-invasive phenotype from WGCNA gene module MEnavajowhite1 from Fig. 6c in the main text.
KCNJ11, ZAR1L, RNU6-4P, RBM22P2, AC019077.1, AC018638.2, AL139120.1, AK4P6, AP003393.1, AC119044.1, AL137191.1, RNU6-94P, AC026356.2, AL354718.3, AC137936.1

REFERENCES AND NOTES

1. O. Veiseh, F. M. Kievit, R. G. Ellenbogen, M. Zhang, Cancer cell invasion: Treatment and monitoring opportunities in nanomedicine. *Adv. Drug Deliv. Rev.* **63**, 582–596 (2011).

2. A. Albini, Y. Iwamoto, H. K. Kleinman, G. R. Martin, S. A. Aaronson, J. M. Kozlowski, R. N. McEwan, A rapid in vitro assay for quantitating the invasive potential of tumor cells. *Cancer Res.* **47**, 3239–45 (1987).

3. Y.-C. Chen, S. G. Allen, P. N. Ingram, R. Buckanovich, S. D. Merajver, E. Yoon, Single-cell migration chip for chemotaxis-based microfluidic selection of heterogeneous cell populations. *Sci. Rep.* **5**, 9980 (2015).

4. C. L. Yankaskas, K. N. Thompson, C. D. Paul, M. I. Vitolo, P. Mistriotis, A. Mahendra, V. K. Bajpai, D. J. Shea, K. M. Manto, A. C. Chai, N. Varadarajan, A. Kontrogianni-Konstantopoulos, S. S. Martin, K. Konstantopoulos, A microfluidic assay for the quantification of the metastatic propensity of breast cancer specimens. *Nat. Biomed. Eng.* **3**, 452–465 (2019).

5. M. Poudineh, M. Labib, S. Ahmed, L. N. M. Nguyen, L. Kermanshah, R. M. Mohamadi, E. H. Sargent, S. O. Kelley, Profiling functional and biochemical phenotypes of circulating tumor cells using a two-dimensional sorting device. *Angew. Chem. Int. Ed. Engl.* **56**, 163–168 (2017).

6. S. P. Desai, S. N. Bhatia, M. Toner, D. Irimia, Mitochondrial localization and the persistent migration of epithelial cancer cells. *Biophys. J.* **104**, 2077–2088 (2013).

7. R. A. Mosig, L. Lin, E. Senturk, H. Shah, F. Huang, P. Schlosshauer, S. Cohen, R. Fruscio, S. Marchini, M. D'Incalci, R. Sachidanandam, P. Dottino, J. A. Martignetti, Application of RNA-seq transcriptome analysis: CD151 is an invasion/migration target in all stages of epithelial ovarian cancer. *J. Ovarian Res.* **5**, 4 (2012).

8. P. Friedl, S. Alexander, Cancer invasion and the microenvironment: Plasticity and reciprocity. *Cell* **147**, 992–1009 (2011).

9. A. G. Clark, D. M. Vignjevic, Modes of cancer cell invasion and the role of the microenvironment. *Curr. Opin. Cell Biol.* **36**, 13–22 (2015).

10. V. Brekhman, G. Neufeld, A novel asymmetric 3D in-vitro assay for the study of tumor cell invasion. *BMC Cancer* **9**, 415 (2009).

11. I. K. Zervantonakis, S. K. Hughes-Alford, J. L. Charest, J. S. Condeelis, F. B. Gertler, R. D. Kamm, Three-dimensional microfluidic model for tumor cell intravasation and endothelial barrier function. *Proc. Natl. Acad. Sci. U.S.A.* **109**, 13515–13520 (2012).

12. J. S. Jeon, S. Bersini, M. Gilardi, G. Dubini, J. L. Charest, M. Moretti, R. D. Kamm, Human 3D vascularized organotypic microfluidic assays to study breast cancer cell extravasation. *Proc. Natl. Acad. Sci. U.S.A.* **112**, 214–219 (2015).

13. D. Truong, J. Puleo, A. Llave, G. Mouneimne, R. D. Kamm, M. Nikkhah, Breast cancer cell invasion into a three dimensional tumor-stroma microenvironment. *Sci. Rep.* **6**, 34094 (2016).

14. Y.-C. Toh, A. Raja, H. Yu, D. van Noort, Y.-C. Toh, A. Raja, H. Yu, D. Van Noort, A 3D microfluidic model to recapitulate cancer cell migration and invasion. *Bioengineering* **5**, 29 (2018).

15. C. Frick, P. Dettinger, J. Renkawitz, A. Jauch, C. T. Berger, M. Recher, T. Schroeder, M. Mehling, Nano-scale microfluidics to study 3D chemotaxis at the single cell level. *PLOS ONE* **13**, e0198330 (2018).

16. W. Han, S. Chen, W. Yuan, Q. Fan, J. Tian, X. Wang, L. Chen, X. Zhang, W. Wei, R. Liu, J. Qu, Y. Jiao, R. H. Austin, L. Liu, Oriented collagen fibers direct tumor cell intravasation. *Proc. Natl. Acad. Sci. U.S.A.* **113**, 11208–11213 (2016).

17. I. A. Eydelnant, B. B. Li, A. R. Wheeler, Microgels on-demand. *Nat. Commun.* **5**, 3355 (2014).

18. M.-Y. Chiang, Y.-W. Hsu, H.-Y. Hsieh, S.-Y. Chen, S.-K. Fan, Constructing 3D heterogeneous hydrogels from electrically manipulated prepolymer droplets and crosslinked microgels. *Sci. Adv.* **2**, e1600964 (2016).

19. B. F. Bender, A. P. Aijian, R. L. Garrell, Digital microfluidics for spheroid-based invasion assays. *Lab Chip* **16**, 1505–1513 (2016).

20. B. A. Nestor, E. Samiei, R. Samanipour, A. Gupta, A. Van den Berg, M. Diaz de Leon Derby, Z. Wang, H. R. Nejad, K. Kim, M. Hoorfar, Digital microfluidic platform for dielectrophoretic patterning of cells encapsulated in hydrogel droplets. *RSC Adv.* **6**, 57409–57416 (2016).

21. I. A. Eydelnant, U. Uddayasankar, B. Li, M. W. Liao, A. R. Wheeler, Virtual microwells for digital microfluidic reagent dispensing and cell culture. *Lab Chip* **12**, 750–757 (2012).

22. R. Fridman, G. Giaccone, T. Kanemoto, G. R. Martin, A. F. Gazdar, J. L. Mulshine, Reconstituted basement membrane (matrigel) and laminin can enhance the tumorigenicity and the drug resistance of small cell lung cancer cell lines. *Proc. Natl. Acad. Sci.* **87**, 6698–6702 (1990).

23. L. C. Kelley, L. L. Lohmer, E. J. Hagedorn, D. R. Sherwood, Traversing the basement membrane in vivo: A diversity of strategies. *J. Cell Biol.* **204**, 291–302 (2014).

24. I. Y. Wong, S. Javaid, E. A. Wong, S. Perk, D. A. Haber, M. Toner, D. Irimia, Collective and individual migration following the epithelial–mesenchymal transition. *Nat. Mater.* **13**, 1063–1071 (2014).

25. P. A. Kenny, G. Y. Lee, C. A. Myers, R. M. Neve, J. R. Semeiks, P. T. Spellman, K. Lorenz, E. H. Lee, M. H. Barcellos-Hoff, O. W. Petersen, J. W. Gray, M. J. Bissell, The morphologies of breast cancer cell lines in three-dimensional assays correlate with their profiles of gene expression. *Mol. Oncol.* **1**, 84–96 (2007).

26. N. Kanwar, P. Hu, P. Bedard, M. Clemons, D. McCready, S. J. Done, Identification of genomic signatures in circulating tumor cells from breast cancer. *Int. J. Cancer* **137**, 332–344 (2015).

27. B. P. Mahadik, T. D. Wheeler, L. J. Skertich, P. J. A. Kenis, B. A. C. Harley, Microfluidic generation of gradient hydrogels to modulate hematopoietic stem cell culture environment. *Adv. Healthc. Mater.* **3**, 449–458 (2014).

28. M. V Kuleshov, M. R. Jones, A. D. Rouillard, N. F. Fernandez, Q. Duan, Z. Wang, S. Koplev, S. L. Jenkins, K. M. Jagodnik, A. Lachmann, M. G. McDermott, C. D. Monteiro, G. W. Gundersen, A. Ma'ayan, Enrichr: A comprehensive gene set enrichment analysis web server 2016 update. *Nucleic Acids Res.* **44**, W90-W97 (2016).

29. A. J. Minn, G. P. Gupta, P. M. Siegel, P. D. Bos, W. Shu, D. D. Giri, A. Viale, A. B. Olshen, W. L. Gerald, J. Massagué, Genes that mediate breast cancer metastasis to lung **436**, 518-524 (2005).

30. S.-Q. Li, N. Su, P. Gong, H.-B. Zhang, J. Liu, D. Wang, Y.-P. Sun, Y. Zhang, F. Qian, B. Zhao, Y. Yu, R. D. Ye, The expression of formyl peptide receptor 1 is correlated with tumor invasion of human colorectal cancer. *Sci. Rep.* **7**, 5918 (2017).

31. X. Chen, X. Cao, X. Sun, R. Lei, P. Chen, Y. Zhao, Y. Jiang, J. Yin, R. Chen, D. Ye, Q. Wang, Z. Liu, S. Liu, C. Cheng, J. Mao, Y. Hou, M. Wang, U. Siebenlist, Y. Eugene Chin, Y. Wang, L. Cao, G. Hu, X. Zhang, Bcl-3 regulates TGFβ signaling by stabilizing Smad3 during breast cancer pulmonary metastasis. *Cell Death Dis.* **7**, e2508 (2016).

32. J. Y. S. Tsang, Y.-B. Ni, S.-K. Chan, M.-M. Shao, Y.-K. Kwok, K.-W. Chan, P. H. Tan, G. M. Tse, CX3CL1 expression is associated with poor outcome in breast cancer patients. *Breast Cancer Res. Treat.* **140**, 495–504 (2013).

33. S. B. Sonne, C. E. Hoei-Hansen, J. E. Nielsen, A. S. Herlihy, A. M. Andersson, K. Almstrup, G. Daugaard, N. E. Skakkebaek, H. Leffers, E. Rajpert-De Meyts, CDH1 (E-cadherin) in testicular germ cell neoplasia: Suppressed translation of mRNA in pre-invasive carcinoma in situ but increased protein levels in advanced tumours. *APMIS* **114**, 549–558 (2006).

34. H. Yuan, M. Yan, G. Zhang, W. Liu, C. Deng, G. Liao, L. Xu, T. Luo, H. Yan, Z. Long, A. Shi, T. Zhao, Y. Xiao, X. Li, CancerSEA: A cancer single-cell state atlas. *Nucleic Acids Res.* **47**, D900-D908 (2019).

35. N. Aceto, A. Bardia, B. S. Wittner, M. C. Donaldson, R. O'Keefe, A. Engstrom, F. Bersani, Y. Zheng, V. Comaills, K. Niederhoffer, H. Zhu, O. Mackenzie, T. Shioda, D. Sgroi, R. Kapur, D. T. Ting,

B. Moy, S. Ramaswamy, M. Toner, D. A. Haber, S. Maheswaran, AR expression in breast cancer CTCs associates with bone metastases. *Mol. Cancer Res.* **16**, 720–727 (2018).

36. N. V. Jordan, A. Bardia, B. S. Wittner, C. Benes, M. Ligorio, Y. Zheng, M. Yu, T. K. Sundaresan, J. A. Licausi, R. Desai, R. M. O'Keefe, R. Y. Ebright, M. Boukhali, S. Sil, M. L. Onozato, A. J. Iafrate, R. Kapur, D. Sgroi, D. T. Ting, M. Toner, S. Ramaswamy, W. Haas, S. Maheswaran, D. A. Haber, HER2 expression identifies dynamic functional states within circulating breast cancer cells. *Nature* **537**, 102–106 (2016).

37. P. Langfelder, S. Horvath, WGCNA: An R package for weighted correlation network analysis. *BMC Bioinformatics* **9**, 559 (2008).

38. L. Cancela, C. L. Hsieh, U. Francke, P. A. Price, Molecular structure, chromosome assignment, and promoter organization of the human matrix Gla protein gene. *J. Biol. Chem.* **265**, 15040-15048 (1990).

39. A. B. Csoka, G. I. Frost, R. Stern, The six hyaluronidase-like genes in the human and mouse genomes. *Matrix Biol.* **20**, 499-508 (2001).

40. J. Lattin, D. A. Zidar, K. Schroder, S. Kellie, D. A. Hume, M. J. Sweet, G-protein-coupled receptor expression, function, and signaling in macrophages. *J. Leukoc. Biol.* **82**, 16-32 (2007).

41. B. Plougastel, T. Jones, J. Trowsdale, Genomic structure, chromosome location, and alternative splicing of the human NKG2A gene. *Immunogenetics* **44**, 286-291 (1996).

42. S. Patowary, E. Alvarez-Curto, T.-R. Xu, J. D. Holz, J. A. Oliver, G. Milligan, V. Raicu, The muscarinic M_3 acetylcholine receptor exists as two differently sized complexes at the plasma membrane. *Biochem. J.* **452**, 303-312 (2013).

43. R. Fobel, C. Fobel, A. R. Wheeler, DropBot: An open-source digital microfluidic control system with precise control of electrostatic driving force and instantaneous drop velocity measurement. *Appl. Phys. Lett.* **102**, 193513 (2013).

44. D. Witters, N. Vergauwe, S. Vermeir, F. Ceyssens, S. Liekens, R. Puers, J. Lammertyn, Biofunctionalization of electrowetting-on-dielectric digital microfluidic chips for miniaturized cell-based applications. *Lab Chip* **11**, 2790–2794 (2011).

45. I. Swyer, R. Fobel, A. R. Wheeler, Velocity saturation in digital microfluidics. *Langmuir* **35**, 5342–5352 (2019).

46. Y. Y. Chen, P. N. Silva, A. M. Syed, S. Sindhwani, J. V. Rocheleau, W. C. W. Chan, Clarifying intact 3D tissues on a microfluidic chip for high-throughput structural analysis. *Proc. Natl. Acad. Sci. U.S.A.* **113**, 14915–14920 (2016).

47. A. M. Bolger, M. Lohse, B. Usadel, Trimmomatic: A flexible trimmer for Illumina sequence data. *Bioinformatics* **30**, 2114–2120 (2014).

48. A. Dobin, C. A. Davis, F. Schlesinger, J. Drenkow, C. Zaleski, S. Jha, P. Batut, M. Chaisson, T. R. Gingeras, STAR: Ultrafast universal RNA-seq aligner. *Bioinformatics* **29**, 15–21 (2013).

49. Y. Liao, G. K. Smyth, W. Shi, featureCounts: An efficient general purpose program for assigning sequence reads to genomic features. *Bioinformatics* **30**, 923–930 (2014).

50. L. McInnes, J. Healy, N. Saul, L. Großberger, UMAP: Uniform manifold approximation and projection. *J. Open Source Softw.* **3**, 861 (2018).

51. M. D. Robinson, D. J. McCarthy, G. K. Smyth, edgeR: A bioconductor package for differential expression analysis of digital gene expression data. *Bioinformatics* **26**, 139-140 (2010).

52. V. Gómez-Rubio, ggplot2 - elegant graphics for data analysis (2nd edition). *J. Stat. Softw.* **77**, 10.18637/jss.v077.b02 (2017).

53. R. L. Blackmon, R. Sandhu, B. S. Chapman, P. Casbas-Hernandez, J. B. Tracy, M. A. Troester, A. L. Oldenburg, Imaging extracellular matrix remodeling in vitro by diffusion-sensitive optical coherence tomography. *Biophys. J.* **110**, 1858–1868 (2016).

54. N. R. Lang, K. Skodzek, S. Hurst, A. Mainka, J. Steinwachs, J. Schneider, K. E. Aifantis, B. Fabry, Biphasic response of cell invasion to matrix stiffness in three-dimensional biopolymer networks. *Acta Biomater*. **13**, 61–67 (2015).